Biophysical Chemistry, 48 (1994) 337–351
Elsevier Science B.V., Amsterdam

BIOCHE 01815

Fluorescence dynamics of diphenyl-1,3,5-hexatriene-labeled phospholipids in bilayer membranes

E.H.W. Pap [a], J.J. ter Horst [a,1], A. van Hoek [b] and A.J.W.G. Visser [a,*]

[a] *Department of Biochemistry, Agricultural University, Dreijenlaan 3, 6703 HA Wageningen (The Netherlands)*
[b] *Department of Molecular Physics, Agricultural University, Dreijenlaan 3, 6703 HA Wageningen (The Netherlands)*

(Received 2 September 1993; accepted in revised form 7 September 1993)

Abstract

A comparative study of the dynamical fluorescence properties of three phosphatidylcholines having a diphenyl-1,3,5-hexatriene (DPH) group attached at different depths from the head group incorporated into membrane vesicles has been carried out. The probes were covalently attached to the sn-2 position of the glycerol part of the phosphatidylcholine via either carboxyl, ethyl or propanoyl links. The vesicles were composed of either dimyristoylphosphatidylcholine or dipalmitoylphosphatidylcholine. The experimental time-resolved polarized fluorescence data of the probes were analysed by two different methods: maximum entropy and global analysis. Distributed fluorescence lifetimes and correlation times of the DPH derivatives were obtained with the maximum entropy method. All DPH derivatives exhibited a bimodal distribution of fluorescence lifetimes with a dependence of the lifetime peak positions on the lipid phase, confirming previous data in the literature. The anisotropic rotational dynamics of the DPH moieties in the membranes could be described by several distributed correlation times. In the fluid phase of the membrane the residual anisotropy of free DPH became very small in contrast with those of the other probes, indicating that restriction of probe rotation is mainly imposed by the molecular geometry of the lipid probes. A two-dimensional analysis using the maximum entropy method demonstrated that both rotational correlation times were associated with the same set of fluorescence lifetimes. Global analysis of the data sets according to the general rotational diffusion model yielded weighted orientational distributions. Unexpectedly, a component of the DPH moiety oriented parallel to the membrane surface was obtained in the orientational distributions of the DPH lipids (as was reported earlier for DPH and TMA-DPH), which seems at variance with the geometric constraints imposed by the headgroups.

Keywords: DPH-phospholipids; Fluorescence lifetime distribution; Rotational correlation-time distribution; Maximum entropy method

1. Introduction

Fluorescence spectroscopy of lipid probe molecules provides us with a valuable tool for studying structure and dynamics of membrane bilayers with the advantage of having a minimal disturbing effect on the membrane. Many time-resolved fluorescence studies (summarized in [1]) on the physical properties of the cylindrically shaped probe diphenyl-1,3,5-hexatriene (DPH) and its charged analogue TMA-DPH have been reported yielding detailed information on the physical state of the phospholipid bilayers. Sev-

* Corresponding author.
[1] Current address: Laboratory of Molecular Dynamics and Spectroscopy, Department of Chemistry, Katholieke Universiteit Leuven, Belgium.

SSDI 0301-4622(93)E0069-H

eral studies distinguished two distinct DPH populations, distributed parallel and perpendicular with respect to the normal of the membrane [2–9]. A better defined orientational distribution would be desirable. To achieve this goal we have used three distinct DPH-labeled phosphatidylcholines with the DPH moieties incorporated at different depths at the sn-2 position (Fig. 1). These DPH lipids are expected to have a more defined orientational distribution and, in addition, they do not significantly perturb the bilayer packing.

We have undertaken a comparative time-resolved fluorescence study of these DPH lipids, including also DPH and TMA-DPH in this comparison. Two methods of analysis of time-resolved data have been employed. The first non a priori method consists of a mathematical description in distribution of relaxation times (both for total fluorescence and for fluorescence anisotropy) using the maximum entropy method (MEM) [10–13]. The physical parameters which can be extracted from this mathematical description of the anisotropy decay are the initial anisotropy (r_0) and the perpendicular rotational diffusion coefficient ($D_\perp$) of this cylindrically symmetrical molecule. Secondly, the polarized time-resolved fluorescence data were also subjected to a global analysis with the (a priori) general diffusion model (r_{g3}) to yield the target parameters $D_\perp$ and the second-rank and fourth-rank order parameters ($\langle P_2 \rangle$ and $\langle P_4 \rangle$) [14,15]. The measurements were performed as a function of temperature by using macroscopically isotropic, small unilamellar vesicles (SUVs) of dimyristoylphosphatidylcholine (DMPC) and dipalmi-

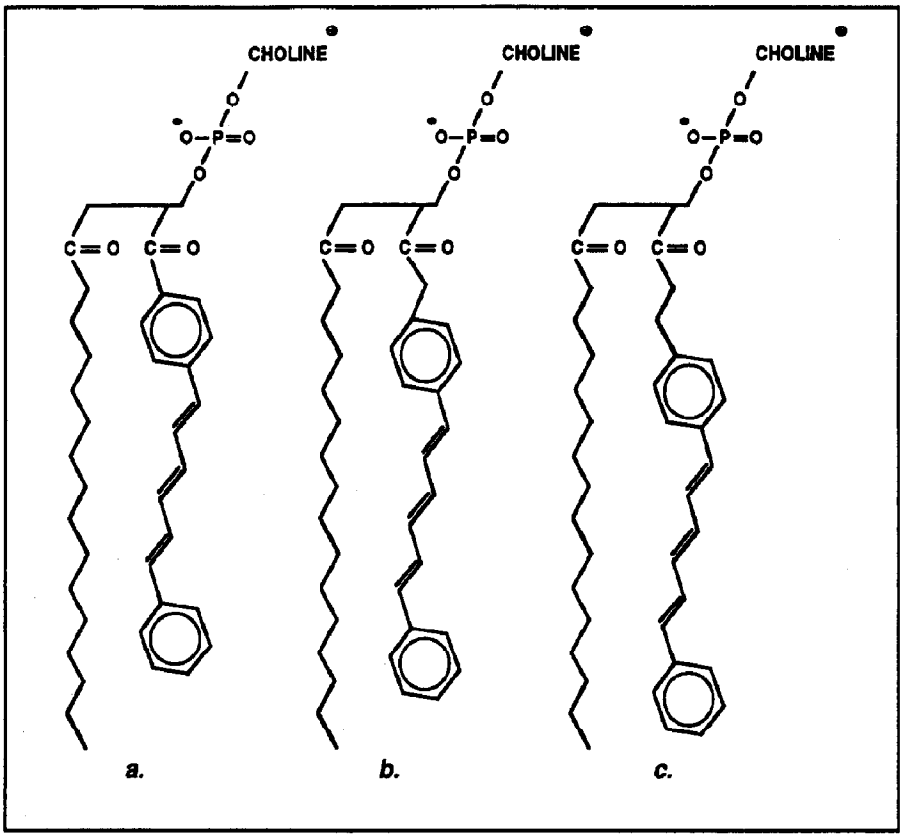

Fig. 1. Chemical structures of the used DPH-labeled phosphatidylcholines. (a) DPHcPC, (b) DPHePC, (c) DPHpPC.

toylphosphatidylcholine (DPPC) with lamellar phase transition temperatures (T_m) of 24°C and 42°C, respectively [16].

2. Materials and methods

2.1. Materials

DMPC and DPPC were purchased from Sigma (St. Louis, MO, USA) and used without further purification. The fluorescent probes DPH, TMA-DPH, DPHpPC and DPH-carboxylic acid were obtained from Molecular Probes (Eugene, OR, USA). DPH-acetic acid was purchased from Lambda (Graz, Austria). The lipid probes DPHePC and DPHcPC were synthesized as described below. The probes were dissolved in absolute ethanol and stored under nitrogen in the dark at −20°C.

2.2. Methods

2.2.1. Synthesis of 2-[3-(diphenylhexatrienyl)-ethyl-3-palmitoyl-L-α-phosphatidylcholine and of 2-[3-(diphenylhexatrienyl)-carboxyl-3-palmitoyl-L-α-phosphatidylcholine

DPHePC and DPHcPC were synthesized essentially as described for sn-2-(pyrenyldecanoyl)-PC by Somerharju and Wirtz [17]. Because of the low solubility of the DPH probes in chloroform, pyridine was used as solvent during the esterification. The DPH-labeled lipids were purified on a silicic acid column, using a methanol gradient in chloroform as eluent. The final yield of the fluorescent phospholipids, based on phosphorous content was about 5%.

2.2.2. Vesicle preparation

SUVs were prepared by injecting 10 μl of a lipid solution (20 m*M* lipid in ethanol) through a Hamilton syringe into 1 mL of a magnetically stirred buffer solution (0.1 M NaCl, 10 mM Tris, pH 8.0) at a temperature 15 degrees higher than the transition temperature of the used phosphatidylcholine species. This procedure produces SUVs having an average diameter of the vesicles at this lipid concentration of 30 nm [18]. The probe:lipid ratio was 1:500 on a molar basis. The total phospholipid content was determined by phosphate analysis according to the method of Rousser et al. [19].

2.2.3. Fluorescence methods

Time-resolved fluorescent measurements were carried out using the time-correlated single-photon counting technique [20]. For excitation with light of 345 nm a frequency-doubled synchronously pumped dye laser (DCM) was used [21]. An electro-optic modulator setup was used to decrease the excitation pulse rate from 76 MHz to 596 kHz. The emission light was collected with a single-photon counting detection system. A combination of a Schott KV399 cutoff filter and Schott 441.7 nm interference filter was used to select the emission wavelength. As a reference compound POPOP (Eastman Kodak Rochester, NY, USA) dissolved in ethanol was used to yield the dynamic instrumental response function of the setup. In the analysis of the polarized fluorescence data, the single exponential reference fluorescence decay time was fixed to a value of 1.35 ns [22]. All measurements consisted of a number of sequences of registration of 10 s parallel and 10 s perpendicular polarized emission. The temperature of the samples in a thermostated cuvet holder was regulated using a temperature controller (Oxford model ITC4). After measuring the fluorescence of a sample the background emission of samples without DPH probes was measured, at one fifth of the time of sample acquisition, and then used for background subtraction. The background emission was always below 1.5% of the total fluorescence of DPH-labeled samples. The data were collected in a multichannel analyzer and after transfer, analyzed on a Silicon Graphics Personal Iris (model 4D35) computer using the commercially available second generation global analysis package (Globals Unlimited™, Urbana, IL, USA) and MEM (Maximum Entropy Data Consultants Ltd., Cambridge, UK).

2.2.4. Maximum entropy method

MEM is able to analyze polarized fluorescence data without any restrictions on number, shape

and position of relaxation time distributions. Since this method of analysis is fully described in Refs. [10–13], we will only briefly describe the principle of the maximum entropy method in relation to our application. The recovery of the distribution of exponentials describing the decay of the fluorescence which is convolved by the shape of the excitation flash, is accomplished by minimizing the χ^2 statistic and maximising the Skilling–Jaynes entropy function [23]. The expression for the parallel and perpendicular intensity components after deconvolving the instrumental response function is given in eqs. (1) and (2). The total fluorescence decay is obtained by summing the parallel ($i_{\parallel}$) and twice the perpendicular ($i_{\perp}$) components

$$i_{\parallel}(t) = \tfrac{1}{3}\int_0^{\infty}\int_0^{\infty}\int_{-0.2}^{0.4}\gamma(\tau, \phi, r_0)\, e^{-t/\tau}\, d\tau\, d\phi\, dr_0 + \tfrac{2}{3}\int_0^{\infty}\int_0^{\infty}\int_{-0.2}^{0.4} r_0\gamma(\tau, \phi, r_0)\, e^{-t/\tau} \times e^{-t/\phi}\, d\tau\, d\phi\, dr_0, \quad (1)$$

$$i_{\perp}(t) = \tfrac{1}{3}\int_0^{\infty}\int_0^{\infty}\int_{-0.2}^{0.4}\gamma(\tau, \phi, r_0)\, e^{-t/\tau}\, d\tau\, d\phi\, dr_0 - \tfrac{1}{3}\int_0^{\infty}\int_0^{\infty}\int_{-0.2}^{0.4} r_0\gamma(\tau, \phi, r_0)\, e^{-t/\tau} \times e^{-t/\phi}\, d\tau\, d\phi\, dr_0, \quad (2)$$

where $\gamma(\tau, \phi, r_0)$ represents the number of fluorophores with lifetime τ, rotational correlation time ϕ and initial anisotropy r_0 [13]. One also is able to recover the distribution pattern of the fluorescence anisotropy given by $r(t)$,

$$r(t) = \frac{i_{\parallel}(t) - i_{\perp}(t)}{i_{\parallel}(t) + 2i_{\perp}(t)}. \quad (3)$$

In case that there is a correlation between τ and ϕ (associative modelling), the complete three-dimensional image given by $\gamma(\tau, \phi, r_0)$ can be resolved from time-resolved polarized fluorescence experiments. In the two-dimensional MEM analysis, assuming a constant r_0, the cross-correlations between lifetimes and rotational correlation times are disclosed [10,13].

If one assumes a priori that there is no correlation between τ and ϕ, (non-associative modelling) the images $\alpha(\tau)$ and $\beta(\phi)$ are independent, and eqs. (1) and (2) can be simplified to

$$i_{\parallel} = \tfrac{1}{3}\int_0^{\infty}\alpha(\tau)\, e^{-t/\tau}\, d\tau \int_0^{\infty}\left[1 + 2\beta(\phi)\, e^{-t/\phi}\right] d\phi, \quad (4)$$

$$i_{\perp} = \tfrac{1}{3}\int_0^{\infty}\alpha(\tau)\, e^{-t/\tau}\, d\tau \int_0^{\infty}\left[1 - \beta(\phi)\, e^{-t/\phi}\right] d\phi. \quad (5)$$

The integrated amplitude $\beta(\phi)$ corresponds to the fundamental anisotropy r_0. When using this separation the time dependence of the anisotropy can be described with the integral

$$r(t) = \int_0^{\infty}\beta(\phi)\, e^{-t/\phi}\, d\phi. \quad (6)$$

In the anisotropy analysis with MEM, this integral is approximated by a sum of n exponentials ($n = 40$ in our analyses) yielding the spectrum of amplitudes β against correlation times ϕ. The rotational diffusion coefficient $D_{\perp}$ is defined as [14]

$$D_{\perp} = \frac{1}{6r_0}\lim_{t\to 0}\frac{\partial r}{\partial t}, \quad (7)$$

where $\partial r/\partial t$ at time zero is calculated from the correlation time spectra according to eq. (8) below:

$$\lim_{t\to 0}\frac{\partial r}{\partial t} = \sum_{i=1}^{n}\frac{\beta_i}{\phi_i}, \quad (8)$$

where the summation is carried out over the whole range (n) of β_i values divided by the corresponding correlation times (ϕ_i). In this calculation $D_{\perp}$ was obtained by assuming an average initial anisotropy of the DPH probes of 0.36.

2.2.5. Global analysis

We also analyzed our experimental data with the rotational diffusion model (r_{g3}) in which the motion of the probe is described as diffusion in an anisotropic environment [14,15]. The parameters of this model are the second-rank and

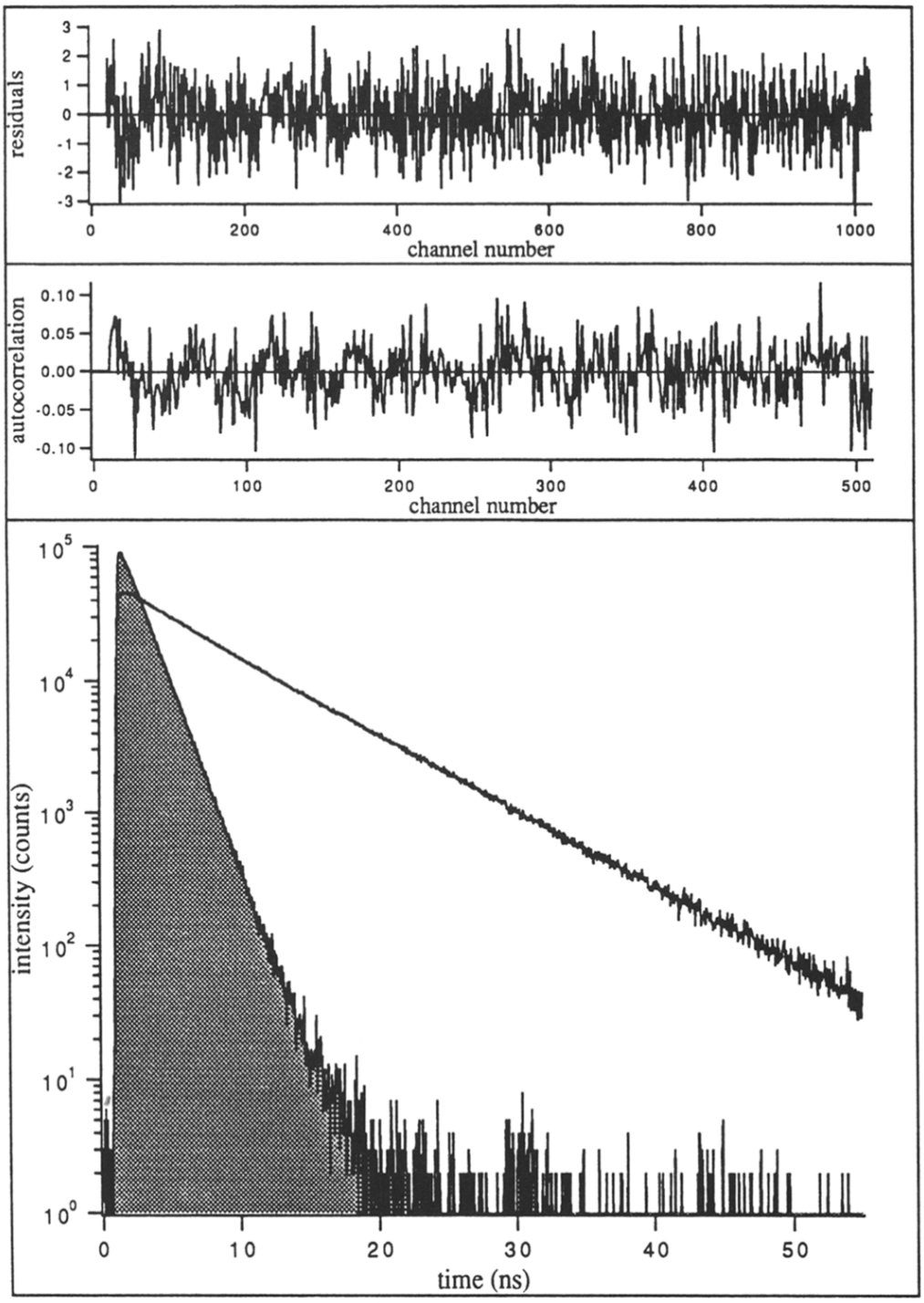

Fig. 2. Experimental total fluorescence decay of DPHpPC in DPPC vesicles at 45°C. Also shown is the response of the POPOP reference compound (shaded). The plots of residuals and autocorrelation of the residuals in the upper panel arise from the fit in a lifetime distribution. These plots are typical for the quality of the fits of all other analyses.

fourth-rank order parameters, $\langle P_2 \rangle$ and $\langle P_4 \rangle$, the diffusion coefficient $D_\perp$ and the initial anisotropy r_0. Multiple experiments of each DPH probe were simultaneously analyzed by linking the initial anisotropy over all temperatures. All fits were subjected to a rigorous error analysis based on an exhaustive search along each parameter axis as to find a minimum χ^2. The error of the fitting parameters was determined according to an F-statistic criterion at the 67% confidence level [24]. Weighted orientational distribution functions were reconstructed from the resolved $\langle P_2 \rangle$ and $\langle P_4 \rangle$ pairs using relationships established by others [6,9,25].

3. Results

3.1. Analysis of fluorescence lifetime distributions

As a typical example the experimental total fluorescence decay of DPHpPC in DPPC vesicles at 45°C is presented in Fig. 2. In all experiments the weighted residuals and autocorrelation functions of the residuals were randomly scattered around zero as illustrated in Fig. 2. The results of a distribution analysis of the fluorescence decay of DPHpPC in DMPC vesicles at several temperatures are shown in Fig. 3. The barycenters of the peaks in the lifetime distribution of the DPH derivatives at several temperatures are presented in Fig. 4. The values of these barycenters agree with published values [3,14,26–29]. All the DPH derivatives show a bimodal distribution, although this is less clear for DPHcPC. The shorter component (denoted τ_1) as well as the longer component (denoted τ_2) are dependent on temperature and physical state of the vesicle (Fig. 3). Because of the low accuracy of τ_1 in the lifetime distribution of DPHcPC, these barycenters have been omitted in Fig. 4. The separation between the peak values of τ_1 and τ_2 decreases from DPH > DPHpPC ≈ DPHePC > DPHcPC ≈ TMA-DPH. The lifetime distributions of the DPH derivatives in DPPC-vesicles are below and above the phase transition temperature (T_m) essentially the same as in DMPC vesicles. When we compare the lifetime distributions of the different DPH

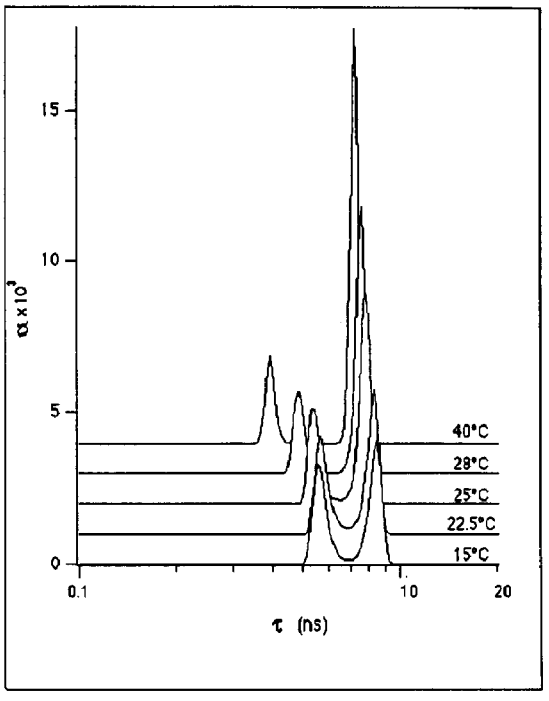

Fig. 3. Temperature dependence of the fluorescence lifetime distribution of DPHpPC in DMPC vesicles. The plots at different temperatures have different offsets which implicates that the ordinate values apply only to the data at 15°C.

derivatives the following conclusions can be drawn:

(i) The widths of the distributions of TMA-DPH and DPHcPC are broader than those of DPH and DPHpPC which might be due to the fact that DPH in the first two probes resides in a region with a large polarity gradient [27].

(ii) The lifetime spectrum of DPHePC is similar to that of DPHpPC, indicating that the dielectric constant near the headgroups is not detectably different within a distance of one C–C bond (≈ 1.8 Å). Differences in barycenters of both probes are within the error margins.

(iii) The lifetime distribution pattern of DPHcPC is shifted to shorter time as compared to that of the other lipid probes. This shift in distribution is probably related to the sensitivity of the fluorescence lifetime of the DPH moiety to substitutions directly in the phenyl group of DPH [30]. All DPH probes exhibit a shortening of the lifetimes with increasing temperature as shown in Figs. 3 and 4, which is consistent with increased

water penetration into bilayers. The relative temperature dependence of the average fluorescence lifetime of the probes located close to the headgroup region of the bilayer (TMA-DPH and DPHcPC) is slightly more marked than that of the other probes (see also [31]). The width of the distribution decreases at higher temperature, which might be a consequence of an increasing rate of exchange between states of slightly different lifetimes within one distribution [27]. During the phase transition the barycenters of both distributed lifetime components of all DPH derivatives shift to shorter times, indicating the sensitivity of the lifetime values to the phase of the lipid bilayer (see also [27,32–34]).

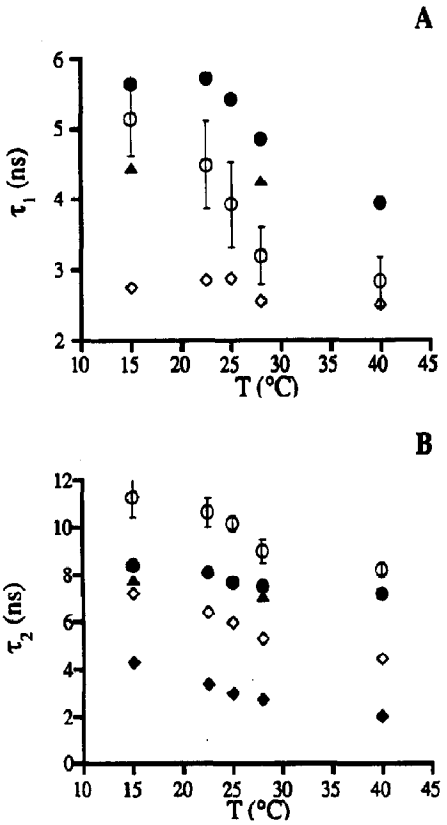

Fig. 4. Temperature dependence of the barycenters of the bimodal fluorescence lifetime distribution of different DPH probes in DPPC bilayers. (A) The shorter fluorescence lifetime τ_1. (B) The longer fluorescence lifetime τ_2. (○) DPH, (●) DPHpPC, (◇) TMA-DPH, (◆) DPHcPC, (▲) DPHePC. In each plot one representative data set is presented with error bars.

3.2. Distribution of correlation times from fluorescence anisotropy decay

An example of the experimental fluorescence anisotropy decay of DPHpPC in DPPC at 45°C is presented in Fig. 5. We have analyzed the polarised fluorescence decay data in terms of a distribution of correlation times and a limiting anisotropy at infinite time (r_∞). For all analyses the weighted residuals and their autocorrelation functions are randomly scattered around zero (see relevant plots). The correlation time spectra of DPHpPC in DMPC as function of temperature are given in Fig. 6. The time-resolved fluorescence anisotropy of the DPH probes at lower temperatures can be described by a unimodal distribution and at higher temperatures by a distribution with at least two components, which can satisfactorily be explained by anisotropic rotation of the DPH moieties using the rotational diffusion model [14,15]. This result agrees with that of discrete exponential analysis [7,27,35,36]. In the inset of Fig. 6 the temperature dependence of the limiting anisotropy r_∞ is given. The contribution of the limiting anisotropy accounts for more than 80% of the initial anisotropy in the gel state of the membrane bilayer. At $T > T_m$, the anisotropy of free DPH tends to relax to a value of r_∞ close to zero, while r_∞ of the other DPH derivatives has still a finite value (Fig. 7A). This behaviour has been explained by assuming a hindered rotation of DPH in lipid bilayers in which the angular barriers are formed by a potential cage consisting of the fatty acid chains in an all-trans configuration, making an angle with the normal of the bilayer [35,36]. When exceeding T_m rotational isomerizations of the fatty acid chains take place causing a drastic increase in rotational freedom in the liquid-crystalline phase. Because the pattern of r_∞ at $T < T_m$ is essentially the same for all probes used, it seems that the limiting anisotropy in the gel phase is only determined by the environment around the fluorescent lipid, and not by intramolecular geometrical restrictions. At higher temperatures the differences between the limiting anisotropies of DPH lipids and free DPH become considerable. Apparently, geometrical constraints or differences in location in the bi-

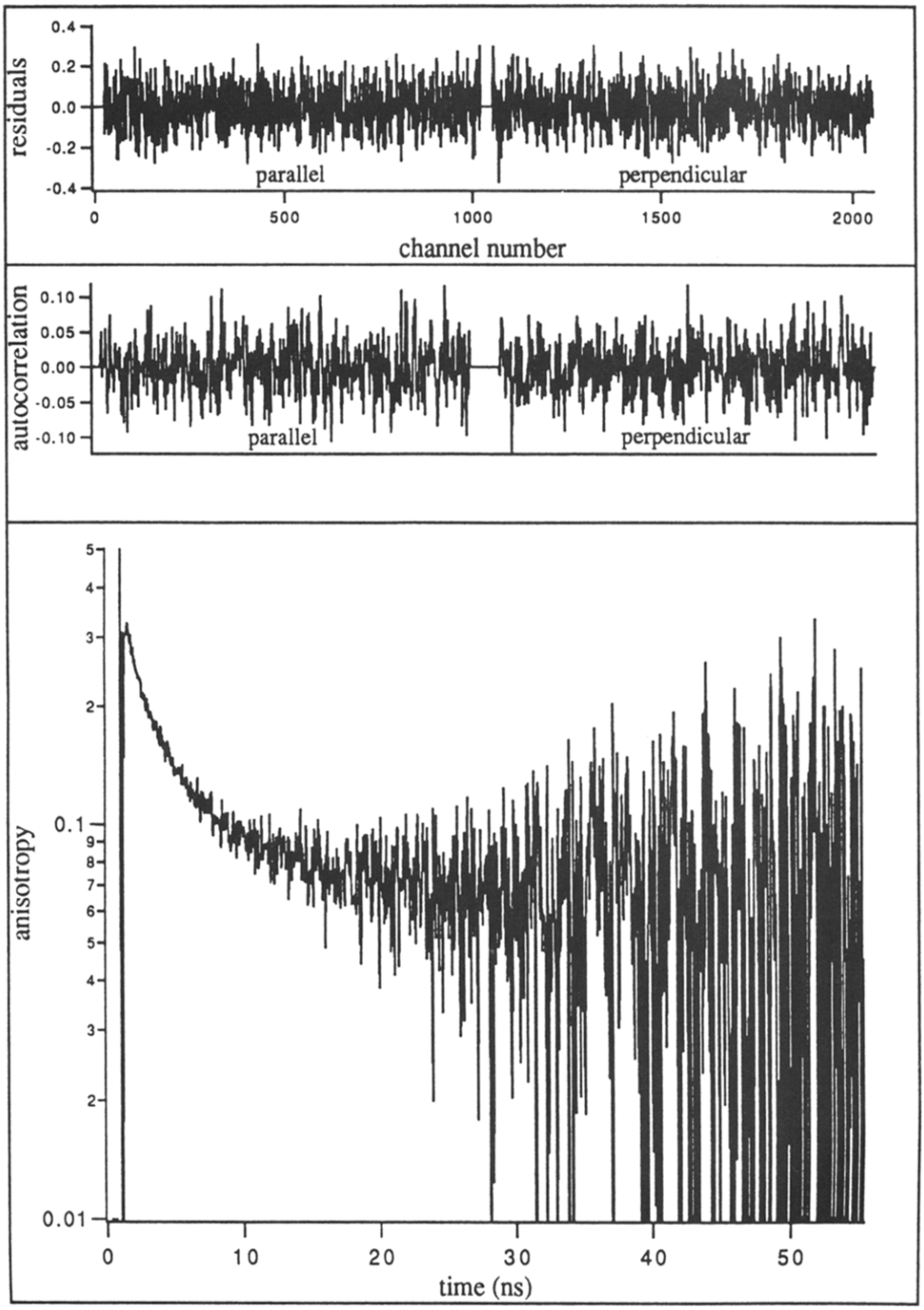

Fig. 5. Experimental, reconstructed fluorescence anisotropy decay of DPHpPC in DMPC vesicles at 28°C. The plots of residuals and autocorrelation of the residuals in the upper panel arise from the fit in a correlation time distribution. These plots are typical for the quality of the fit of all other analyses.

layer become relatively more important in determining the limiting anisotropy in fluid membranes. The r_∞ of DPHcPC and TMA-DPH is at $T \geqslant T_m$ significantly larger than that of DPHePC and DPHpPC. In Fig. 7B and C the barycenters of the main distributed correlation time and the integrated amplitude are given as function of temperature (barycenters of the shorter distributed correlation time could not be determined accurately). The barycenters move to shorter time scale at higher temperatures, which can be explained by faster restricted DPH movements. The barycenters of the main distributed correlation times of the DPH derivatives in DMPC and DPPC vesicles at equal temperatures are essentially the same, while the r_∞ differs largely at temperatures between 20°C and 45°C, which is an obvious consequence of the differences in phase of the two membrane bilayers. The perpendicular diffusion coefficients ($D_\perp$) of the DPH probes in DMPC vesicles, calculated with eqs. (7) and (8), are presented in Table 1. In this approach $D_\perp$ is considered to be an average diffusion coefficient of all chromophores in the

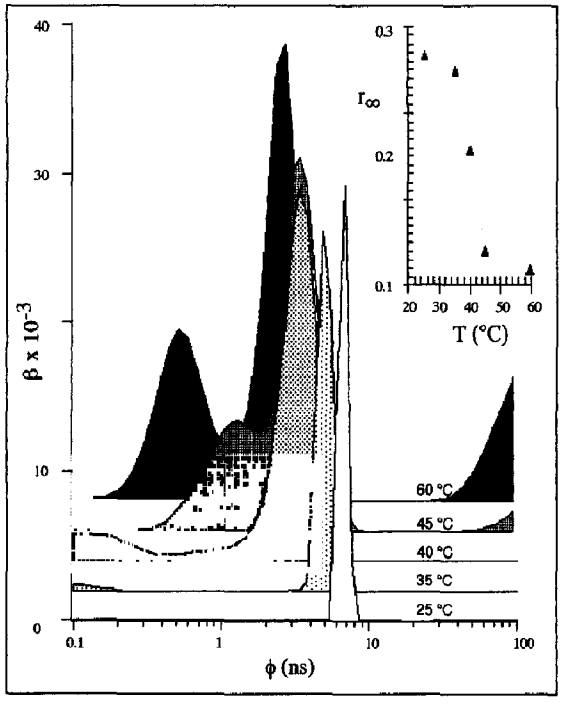

Fig. 6. Temperature dependence of the correlation-time distribution of DPHpPC in DPPC vesicles as obtained with a non-associative MEM analysis. The distributions have different offset values, which implicates that the ordinate values apply only to the data at 25°C. The temperature dependence of the anisotropy at limiting time (r_∞) is presented in the inset.

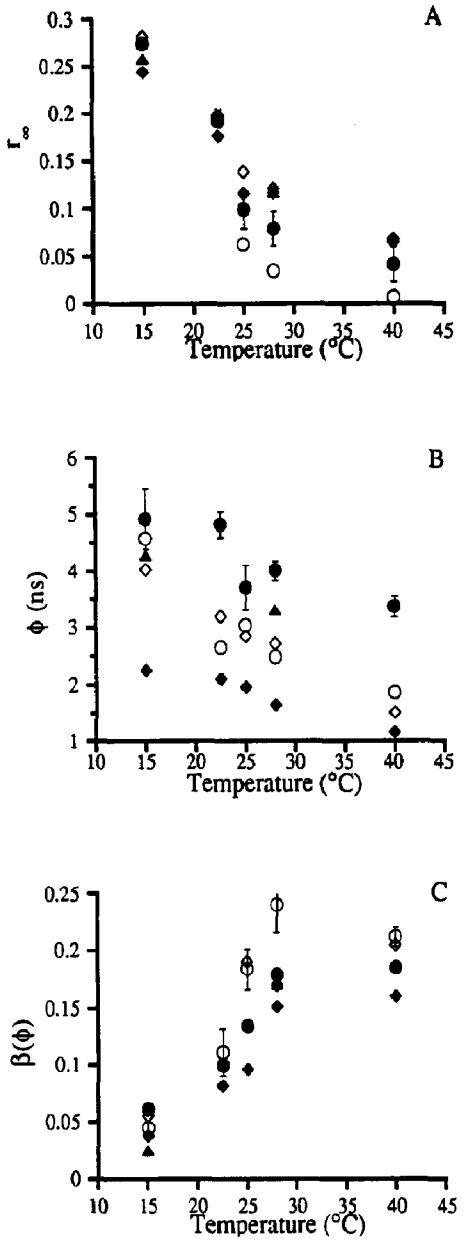

Fig. 7. Temperature dependence of r_∞ (A) and the barycenter (B) and contribution (C) of the main peak in the correlation-time distribution of different DPH probes in DMPC bilayers. (○) DPH, (●) DPHpPC, (◇) TMA-DPH, (◆) DPHcPC, (▲) DPHePC. In each plot one representative data set is presented with error bars.

membrane. The $D_\perp$ values of DPH and TMA-DPH agree rather well with those found by others using discrete exponential analysis [6–8]. The results in Table 1 show that the $D_\perp$ values are considerably smaller for the DPH lipids than for DPH; $D_\perp$ increases in the following order: DPHcPC ≈ TMA-DPH < DPHePC < DPHpPC < DPH. An increase in temperature accelerated the depolarizing motions of the probes in each of the vesicle systems examined. An abrupt change in rate of diffusion was observed during the phase transition for the probes DPH and DPHpPC. For the other probes the changes were more gradual.

3.3. Two-dimensional maximum entropy analysis

All experimental results were further analyzed with a two-dimensional maximum entropy analysis in which the associative behaviour between the fluorescence lifetimes and the rotational correlation times was investigated. As a typical example the results of the analysis of DPHpPC in DMPC at 40°C is presented in Fig. 8. The pattern clearly displays the two lifetime components centred at their true positions along the τ axis (τ_1 = 3.7 and τ_2 = 7.6 ns). Along the ϕ axis we can see the two separated correlation-time peaks associated with τ_1 and τ_2, next to the limiting anisotropy at $\phi = \infty$. Three conclusions from these two-dimensional analyses can be drawn:

(i) The two correlation-time peaks share the same fluorescence lifetimes. The association of the resolved correlation-time peaks with both lifetimes is ambiguous due to iso-kappa interference [10,13]. The four peaks A, B, C and D in Fig. 8 belong to two different iso-kappa curves and three combinations A + D, B + C or A + B + C + D accurately fit the data, only the relative proportion of these peaks being changed. Additional information is needed to resolve this ambiguity.

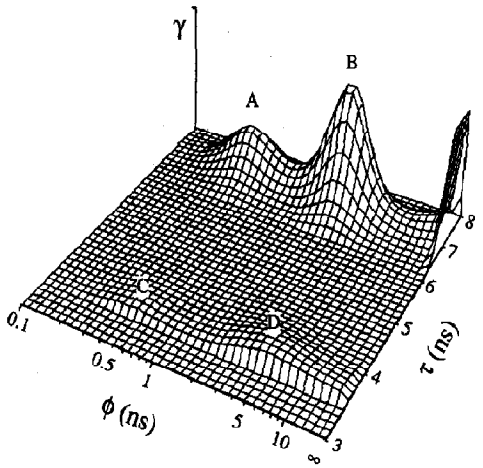

Fig. 8. A three-dimensional plot (τ, ϕ, γ) for DPHpPC in DMPC vesicles at 40°C. The ϕ axis extends between 0.1 and 20 ns. Infinite time scale ($\phi \to \infty$) is indicated at the last point of this axis.

(ii) The main lifetime τ_2, associated with the correlation-time peaks A and B, is in most experiments slightly ($\leqslant 1$ ns) shorter than the fluorescence lifetime associated with r_∞ (see Fig. 8). Simulations (results not shown) in which both correlation-time peaks and r_∞ were associated with the main lifetime peak τ_2, indicated that this difference in lifetimes could be satisfactorily explained by the fact that at long times the observed anisotropy is dominated by the species with the longest lifetime [37].

(iii) None of the analyses demonstrated an association of the limiting anisotropy term with the shorter lifetime τ_1.

Table 1

Temperature dependence of the perpendicular rotational diffusion coefficient (ns^{-1}) of the DPH probes in DMPC vesicles. $D_\perp$ was calculated from the correlation time distributions (obtained from MEM) using eqs. (7) and (8)

T (°C)	DPHpPC	DPHePC	DPHcPC	DPH	TMA-DPH
15	0.002	0.004	0.006	0.023	0.006
22.5	0.016		0.026	0.018	0.027
25	0.071		0.049	0.152	0.048
28	0.097	0.082	0.061	0.163	0.068
40	0.118		0.132	0.198	0.138

3.4. Weighted orientational distribution from global analysis of fluorescence anisotropy decay

In addition to the mathematical approach, the experimental fluorescence anisotropy decays were globally analyzed using the r_{g3} model (see section 2.2). To obtain optimal fits, the order parameters

Table 2

Results of global analysis of the data sets of the DPH probes in DMPC vesicles at various temperatures using the r_{g3} model. The numbers within the parentheses correspond to the errors as determined from a rigorous error analysis at a 67% confidence level. In the analysis the initial anisotropy of each lipid probe was globally linked

Probe	T (°C)	$\langle P_2 \rangle$	$\langle P_4 \rangle$	$D_\perp$ (ns^{-1})	global r_0	global χ^2
DPH	15	0.89	0.79	0.06		
		(0.87–0.9)	(0.72–0.83)	(0.04–0.09)		
	22.5	0.72	0.64	0.12		
		(0.71–0.74)	(0.62–0.72)	(0.08–0.18)		
	25	0.44	0.47	0.23	0.350	1.09
		(0.41–0.46)	(0.42–0.56)	(0.16–0.38)		
	28	0.34	0.41	0.28		
		(0.32–0.35)	(0.39–0.46)	(0.19–0.40)		
	40	0.17	0.11	0.43		
		(0.13–0.18)	(0.07–0.16)	(0.36–0.49)		
TMA-DPH	15	0.89	0.80	0.03		
		(0.88–0.90)	(0.74–0.82)	(0.02–0.08)		
	22.5	0.75	0.62	0.11		
		(0.73–0.77)	(0.59–0.70)	(0.09–0.16)		
	25	0.65	0.52	0.15	0.355	1.24
		0.62–0.68	(0.50–0.62)	(0.13–0.31)		
	28	0.61	0.46	0.20		
		(0.56–0.66)	(0.41–0.51)	(0.16–0.28)		
	40	0.49	0.18	0.30		
		(0.45–0.55)	(0.13–0.24)	(0.28–0.38)		
DPHpPC	15	0.86	0.77	0.03		
		(0.68–0.91)	(0.74–0.84)	(0.02–0.08)		
	22.5	0.76	0.66	0.06		
		(0.66–0.8)	(0.62–0.77)	(0.05–0.1)		
	25	0.68	0.63	0.10	0.361	1.09
		(0.64–0.71)	(0.61–0.68)	(0.07–0.15)		
	28	0.63	0.56	0.11		
		(0.56–0.64)	(0.51–0.63)	(0.08–0.21)		
	40	0.53	0.43	0.15		
		(0.49–0.55)	(0.38–0.52)	(0.13–0.30)		
DPHePC	15	0.84	0.77	0.03	0.356	1.23
		(0.81–0.89)	(0.74–0.83)	(0.02–0.08)		
	28	0.57	0.53	0.21		
		(0.51–0.6)	(0.49–0.58)	(0.14–0.37)		
DPHcPC	15	0.86	0.73	0.07		
		(0.68–0.92)	(0.72–0.82)	(0.05–0.10)		
	22.5	0.77	0.59	0.12		
		(0.69–0.80)	(0.53–0.66)	(0.09–0.24)		
	25	0.71	0.50	0.17	0.355	1.29
		(0.63–0.74)	(0.47–0.59)	(0.10–0.36)		
	28	0.64	0.40	0.28		
		(0.61–0.66)	(0.35–0.48)	(0.23–0.45)		
	40	0.45	0.13	0.49		
		(0.43–0.53)	(0.96–0.19)	(0.42–0.67)		

$\langle P_2 \rangle$, $\langle P_4 \rangle$ and the diffusion constant $D_\perp$ were associated with two discrete lifetimes. These fluorescence lifetimes were obtained from a separate analysis of the total fluorescence decay. The lifetime values obtained approached those of the barycenters from the lifetime distributions (see section 3.1). The initial anisotropy for each probe was linked over experiments at all temperatures. The results of the global analysis are presented in Table 2. The ambiguity of the solution for $\langle P_4 \rangle$ was investigated for DPHpPC in DMPC at 40°C. Although two minima in the dependence of the χ^2 on the value of $\langle P_4 \rangle$ were obtained (data not shown), the χ^2 minimum at $\langle P_4 \rangle = 0.4$ ($\chi^2 = 1.06$) is lower than the minimum at $\langle P_4 \rangle = -0.2$ ($\chi^2 = 1.43$). As expected, both $\langle P_2 \rangle$ and $\langle P_4 \rangle$ of all derivatives decrease with temperature. At temperatures below T_m, the $\langle P_2 \rangle$ and $\langle P_4 \rangle$ values of the different DPH compounds are almost equal, while at temperatures above T_m differences in $\langle P_2 \rangle$ and $\langle P_4 \rangle$ values become pronounced. It is hard to explain the differences between the estimates for the diffusion coefficient $D_\perp$ obtained by MEM (Table 1) and the r_{g3} model (Table 2). One possibility might be that the value of the initial anisotropy, which is determined differently in both programs, has a strong effect on the diffusion coefficient values. The value of the initial anisotropy is determined in the MEM analysis for each experiment individually, while in the r_{g3} analysis it is determined globally from several experiments. The real nature of the difference remains to be investigated systematically. Plots of the weighted orientational distribution of probe molecules against the angle of the emission dipole moment θ with the membrane normal could be constructed from the $\langle P_2 \rangle$ and $\langle P_4 \rangle$ values [6,9,25]. These plots contain information about the angular displacement which is determined by both sterical and geometrical constraints. An example of such a plot for the three DPH lipids is given in Fig. 9. The weighted orientational distributions for the DPH derivatives indicate that the reorientational freedom is restricted both in the hydrophobic core and at the bilayer–water interface. The width of the weighted distribution of DPHpPC and DPHePC is smaller than that of DPHcPC (see Fig. 9), DPH and TMA-DPH (data not shown) indicating that DPH attached to the former two lipids has a narrower angular distribution around the membrane normal. The weighted orientational distributions of the DPH derivatives show a considerable sensitivity to temperature (data not shown). The effect of increasing temperature on the weighted distribution patterns leads us to distinguish three effects:

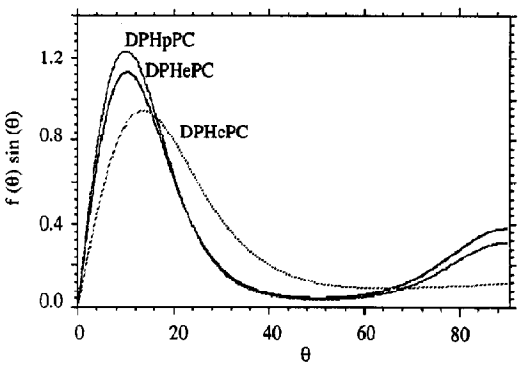

Fig. 9. The weighted orientational distribution $f(\theta))\sin(\theta)$ for DPHpPC, DPHePC and DPHcPC in DPPC vesicles at 45°C. The area under the curve represents the probability of finding the probe at a certain angle.

(i) The distribution shows broadening.

(ii) A shift of the most populated angle in the distribution from shorter values to longer ones. Both effects indicate a decrease of acyl chain ordering.

(iii) A shift of the orientation in favour of alignment of the DPH fluorophore perpendicular to the acyl side chains. This shift was also observed by other workers for DPH [2–8] and TMA-DPH [7,9]. At 60°C in DPPC, the hydrophobic core is even so fluid that DPH rotates almost isotropically, while the other DPH derivatives still have an appreciable distribution minimum between $\theta = 30°$ and $\theta = 70°$, and hence consist of a heterogeneous probe population of anisotropically rotating probes. As shown in Fig. 9 a significant population of DPHpPC and DPHePC molecules is oriented parallel to the plane of the DMPC bilayer at 28°C. This bimodal distribution is less clear and broader for DPHcPC. This remarkable result is due to a relatively high contribution of $\langle P_4 \rangle$ (Table 2). Unexpectedly, the weighted orientational distributions of both

TMA-DPH and DPHcPC are broader and shifted to longer angles than those of DPHePC and DPHpPC. The relatively high position of DPH in the hydrocarbon region of the former probes might affect the heterogeneity in orientation angles. Because the rotational freedom experienced by the DPH portion of the lipids is an effect of both lipid environmental and intramolecular motional restrictions, one would predict that the DPH moiety of DPHcPC and TMA-DPH is more hindered than DPHpPC. It is unclear which two factors determine the differences in the weighted orientational distributions.

No significant differences could be detected in the weighted distribution functions of the DPH derivatives in DMPC compared with those in DPPC at equal temperature and lipid phase.

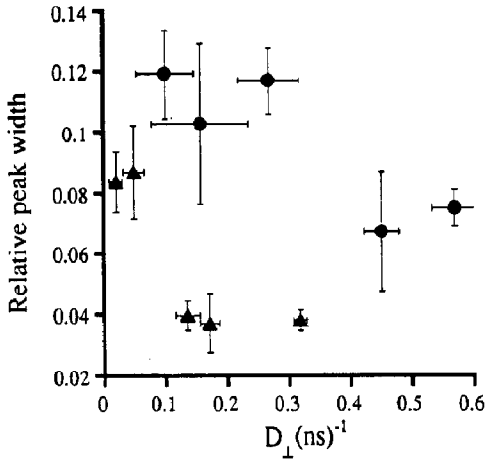

Fig. 10. The rotational diffusion coefficient ($D_\perp$) versus the relative peak half width ($\Delta\tau/\tau$) of the longer lifetime component (τ_2) of DPH (●) and DPHpPC (▲) in DPPC vesicles at various temperatures. Presented are averages with standard errors of values (obtained by MEM) of duplicate experiments.

4. Discussion

4.1. Distribution width

In general the width of a distribution depends on the number of slightly different environmental substates of probe molecules in the membrane and on the rate of exchange between those states. Since all time-resolved fluorescence experiments were carried out using the same total integrated intensity, we can compare the widths of the distributions of different samples. The width of the lifetime distribution depends on temperature and lipid bilayer phase (see also [27]). In Fig. 10 the rotational diffusion coefficient $D_\perp$, which is a measure for the (perpendicular) rotational exchange rate, is plotted against the relative width of τ_2 for DPHpPC and free DPH in DPPC at several temperatures. Although the uncertainty in the points is large, it is evident that the dependencies of the distribution width on $D_\perp$ is different for both DPH molecules. In case of DPHpPC the plot is shifted to lower values. From this it can be concluded that DPH is more heterogeneously distributed in the lipid bilayer than DPHpPC.

4.2. Lifetime and correlation time distributions

The fluorescence decay of the DPH probes in lipid bilayers is described by a bimodal distribution. In chloroform we observed also a bimodal lifetime distribution for DPH and DPHpPC, although the contribution of τ_1 to the fluorescence relaxation is only 6%–12% (results not shown). Several explanations for the physical origin of the shorter lifetime component have been summarised by Lentz [1]. A new viewpoint has recently been given by Brand and co-workers [38]. A double exponential character of the fluorescence decay is expected on the basis of an orientational dependence of the radiative decay rate in optically anisotropic systems. Because we observed also a bimodal lifetime distribution of DPH in isotropic systems (unpublished observations) this phenomenon can not be the only mechanism causing the complex fluorescence relaxation. The ratio of the integrated amplitude, $\alpha(\tau_1)/\alpha(\tau_2)$, varied upon changing the state of the membrane. If two different probe environments would be responsible for the bimodal fluorescence relaxation, both populations would exist at each temperature, in fluid and gel-phase of either DMPC and DPPC membranes.

The two-dimensional MEM analyses of all data sets showed that r_∞ is not associated with the

shorter lifetime component τ_1, indicating that the anisotropic behaviour of chromophores associated with τ_2 is different from the behaviour of those responsible for τ_1. Non-associative fluorescence anisotropy data analysis as applied in the one-dimensional MEM analysis or r_{g3} global analysis, is therefore a first-order approximation. Excitation and emission wavelength dependence of the ratio $\alpha(\tau_1)/\alpha(\tau_2)$ might provide information on the possibility of photoproducts or on the presence of two energetically close excited states [39] as the origin of the shorter lifetime component.

At higher temperatures the anisotropy decay of the DPH derivatives is mathematically described by at least two distributed components of rotational correlation times, next to a limiting anisotropy term. This behaviour is expected in the r_{g3} model (three exponentials and a constant term) in which the preexponential factors are dependent on the actual values of $\langle P_2 \rangle$ and $\langle P_4 \rangle$ and the relaxation times on $\langle P_2 \rangle$, $\langle P_4 \rangle$ and $D_\perp$.

4.3. Weighted orientational distribution of the DPH lipids

According to the results of the fits to the rotational diffusion model, all DPH derivatives have a significant population of probe molecules oriented perpendicular with respect to the normal of the membrane. This result is in contradiction with the current physical model of intrinsically oriented DPH lipids in which it is assumed that the DPH moiety is located in the hydrocarbon region oriented parallel to the acyl chains of the bilayer. Although the uncertainty in the value of $\langle P_4 \rangle$ is large (Table 2), attempts to force the $\langle P_4 \rangle$ values down to values necessary for a unimodal orientational distribution gave according to the F-statistic criterion (see section 2.2), an unacceptable rise in χ^2 values. It is worth noting that the less optimal fit with a negative $\langle P_4 \rangle$ solution (see section 3.4) predicts a physically more consistent unimodal distribution of DPH lipids (see also [8]). Either the r_{g3} model or the physical description of motional restriction of intrinsically oriented probes should be further investigated. The parameters used in the r_{g3} model reflect average properties (rotational dynamics and angular barriers) experienced by all probe molecules. With this assumption a bimodally oriented population of probe molecules is found (Fig. 9). The limitation of the r_{g3} approach can be envisioned by considering that both populations probably consist of probe molecules with different order and diffusion properties. Since the fluorescence lifetimes are hardly dependent on the lipid environment, one is not able to separate both populations on the basis of fluorescence lifetimes. On the other hand it has been shown with molecular dynamics simulations [40] that the overall structure of the membrane shows considerable disorder. If there is a population with the DPH moiety oriented parallel to the membrane plane, these fluorophores are probably not located very high in the hydrocarbon zone, because one would expect a shortening of the average fluorescence lifetime of these chromophores [27], which is not observed.

4.4. DPH lipids

Comparing the fluorescence and anisotropy relaxations of the different DPH-labeled lipids we can conclude that the substitution of the carbonyl group directly to the phenyl ring of DPH (DPHcPC) strongly influences the photophysical properties like observed with TMA-DPH. All distributions are broader than those of DPHePC or DPHpPC, indicating a less defined, heterogeneous environment. On the other hand, the total fluorescence properties and anisotropic behaviour of DPHePC and DPHpPC are very similar. From a comparison of the fluorescence lifetime distributions and weighted orientational distributions of DPHpPC and DPHePC with those of DPH, we can conclude that the DPH lipids exhibit more defined emission properties (sharper lifetime peaks), slower rotational diffusion and narrower angular distributions around the membrane normal.

Acknowledgement

This research was supported by the Netherlands Foundation of Biophysics with financial aid

of the Netherlands Organisation for Scientific Research (NWO).

Appendix

Abbreviations. DCM: 4-dicyanomethylene-2-methyl-6-(*p*-dimethyl-aminostyryl)-4H-pyran; DMPC: dimyristoylphosphatidylcholine; DPPC: dipalmitoylphosphatidylcholine; DPH: 1,6-diphenyl-1,3,5-hexatriene; DPHcPC: 2-[3-(diphenylhexatrienyl)-carboxyl]-3-palmitoyl-L-α-phosphatidylcholine; DPHePC: 2-[3-(diphenylhexatrienyl)-ethyl]-3-palmitoyl-L-α-phosphatidylcholine; DPHpPC: 2-[3-(diphenylhexatrienyl)-propanoyl]-3-palmitoyl-L-α-phosphatidylcholine; MEM: maximum entropy method; POPOP: 1,4-bis[2-(5-phenyloxazolyl)]benzene; r_{g3}: general rotational diffusion model; SUVs: small unilamellar vesicles; TMA-DPH: 1-[4-(trimethylamino)phenyl]-6-phenyl-1,3,5-hexatriene.

References

1 B.R. Lentz, Chem. Phys. Lipids 50 (1989) 171–1901.
2 G. van Ginkel, H. van Langen and Y.K. Levine, Biochimie 71 (1989) 23–32.
3 G. Deinum, H. van Langen, G. van Ginkel, Y.K. Levine, Biochemistry 27 (1988) 852–860.
4 R.P.H. Kooyman, M.H. Vos and Y.K. Levine, Chem Phys. 81 (1983) 461–472.
5 M.H. Vos, R.P.H. Kooyman and Y.K. Levine, Biochem. Biophys. Res. Commun. 116 (1983) 462–468.
6 M. Ameloot, H. Hendrickx, W. Herreman, H. Pottel, F. van Cauwelaert and W. van der Meer, Biophys. J. 46 (1984) 525–539.
7 L. Best, E. John and F. Jähnig, Eur. Biophys. J. 15 (1987) 87–102.
8 S. Wang, J.M. Beechem, E. Gratton and M. Glaser, Biochemistry 30 (1991) 5565–5572.
9 H. van Langen, Y.K. Levine, M. Ameloot and H. Pottel, Chem. Phys. Letters 140 (1987) 394–400.
10 M. Gentin, M. Vincent, J.C. Brochon, A.K. Livesey, N. Cittanova and J. Gallay, Biochemistry 29 (1990) 10405–10412.
11 Å.K. Livesey, and J.C. Brochon, Biophys. J. 52 (1987) 693–706.
12 F. Mérola, R. Rigler, A. Holmgren and J.C. Brochon, Biochemistry 28 (1989) 3383–3398.
13 J.C. Brochon, F. Mérola and A.K. Livesey, in: Synchrotron radiation and dynamic phenomena (American Institute of Physics, New York, 1992) pp. 435–452.
14 W. van der Meer, H. Pottel, W. Herreman, M. Ameloot, H. Hendrickx and H. Schröder, Biophys. J. 46 (1984) 515–523.
15 A. Szabo, J. Chem. Phys. 81 (1984) 150–167.
16 M.D. Houslay and K.K. Stanley, in: Dynamics of biological membranes (Wiley, New York, 1982) p. 54.
17 P.J. Somerharju and K.W.A. Wirtz, Chem. Phys. Lipids 30 (1982) 81–91.
18 J.M.H. Kremer, M.W.J. v.d. Esker, C. Pathmamanoharan and P.H. Wiersema, Biochemisty 16/17 (1977) 3932–3935.
19 G. Rousser, S. Fleischer and A. Yamamoto, Lipids 5 (1970) 494–496.
20 D.V. O'Connor and D. Philips, Time-correlated single photon counting (Academic Press, London, 1984).
21 A. van Hoek, K. Vos and A.J.W.G. Visser, J. Quantum Electron. QE-23 (1987) 1812–1820.
22 K. Vos, A. van Hoek and A.J.W.G. Visser Eur. J. Biochem. 165 (1987) 55–63.
23 E.T. Jaynes, Trans. Biomed. 4 (1968) 227.
24 J.M. Beechem, E. Gratton, M. Ameloot, J.R. Knutson and L. Brand in: Topics in Fluorescence Spectroscopy, ed. Vol. 2, J.R. Lakowicz (Plenum Press, New York, 1991) pp. 241–305.
25 P.J. Berne, P. Pechukas and G.D. Harp, J. Chem. Phys. 49 (1968) 3125–3129.
26 R.A. Parente and B.R. Lentz, Biochemistry 24 (1985) 6178–6185.
27 R. Fiorini, M. Valentino, S. Wang, M. Glaser and E. Gratton, Biochemistry 26 (1987) 3864–3870.
28 L.A. Chen, R.E. Dale, S. Roth and L. Brand, J. Biol. Chem. 252 (1977) 2163–2169.
29 C.R. Mateo, M.P. Lillo, Gonzalez-Rodriguez and A.U. Acuña, Eur. Biophys. J. 20 (1991) 41–52.
30 P.C. Alford and T.F. Palmer, Chem. Phys. Letters 86 (1982) 248–253.
31 M. Straume and B.J. Litman, Biochemistry 26 (1987) 5113–5120.
32 D.A. Barrow and B.R. Lentz, Biophys. J. 48 (1985) 221–234.
33 R.D. Klausner, A.M. Kleinfeld, R.L Hoover and M.J. Karnovsky, J. Biol. Chem. 255 (1980) 1286–1295.
34 T. Parasassi, F. Conti, M. Glaser and E. Gratton, J. Biol. Chem. 259 (1984) 14011–14017.
35 R.E. Dale, L.A. Chen and L. Brand, J. Biol. Chem. 252 (1977) 7500–7510.
36 L. Davenport, J.R. Knutson and L. Brand, Biochemistry 25 (1986) 1811–1816.
37 A. Ruggiero and B. Hudson, Biophys. J. 55 (1989) 1125–1135.
38 D. Toptygin, J. Svobodova, I. Konopasek and L. Brand, J. Chem. Phys. 96 (1992) 7919–7930.
39 C. Rullière and A. Declémy, Chem. Phys. Letters 135 (1987) 213–218.
40 E. Egberts and H.J.C. Berendsen, J. Chem. Phys. 89 (1988) 3718–3732.